GeoScienceEd *7(1) (2026)*

Jurnal Pendidikan, Sains, Geologi, dan Geofisika

http://jpfis.unram.ac.id/index.php/GeoScienceEdu/index

Stability Does Not Guarantee Accuracy: CFL-Compliant 1D Acoustic FDTD and Its Consequences for Near-Surface Layered Modeling

Ruhul Firdaus[1*], Gestin Mey Ekawati[1]

[1] Institut Teknologi Sumatera (ITERA), Geophysical Engineering Department, Lampung, Indonesia.

DOI: https://doi.org/10.29303/goescienceed.v7i1.1693

Article Info:
Received : 04 December 2025
Revised : 20 December 2025
Accepted : 13 January 2026
Published : 28 February 2026

Correspondence:

Ruhul Firdaus

Phone : +6282178716641

Abstract: Explicit finite-difference time-domain (FDTD) solvers for the 1D acoustic wave equation are routinely configured by enforcing the Courant–Friedrichs–Lewy (CFL) stability limit. In near-surface settings, this practice can create a false sense of model fidelity because stability constrains time stepping but does not control phase and amplitude errors induced by numerical dispersion. This report isolates the gap between stable time marching and accurate waveform synthesis in layered, strongly contrasting near-surface media. Beyond the well-known stability–accuracy distinction, the specific contribution is a reproducible near-surface verification workflow that couples a transfer-matrix stratified benchmark with controlled bandwidth variation at fixed CFL and converts the resulting waveform misfits into an explicit dispersion budget and pass–fail acceptance gate. The intended deliverable is an independent verification note that demonstrates, with quantitative evidence, that CFL compliance is necessary for stability but insufficient for accuracy, and that near-surface forward modeling requires an explicit dispersion budget expressed in points per minimum wavelength and validated by waveform misfit diagnostics.

Keywords: FDTD; CFL Condition; Numerical Dispersion; Waveform Accuracy; Near Surface Modeling

Citation: Firdaus, R., & Ekawati, G. M. (2026). Stability Does Not Guarantee Accuracy: CFL-Compliant 1D Acoustic FDTD and Its Consequences for Near-Surface Layered Modeling. *Jurnal Pendidikan, Sains, Geologi, Dan Geofisika (GeoScienceEd Journal)*, *7*(1), 750–756. https://doi.org/10.29303/goescienceed.v7i1.1693

Introduction

Near-surface geophysical modeling is characterized by short wavelengths, strong impedance contrasts, and prominent surface-related reverberations. These features make forward modeling sensitive to discretization error even in 1D layered settings. Explicit FDTD is attractive because it is simple, scalable, and widely used (Kelly et al., 1976). However, practical configuration is often treated as a stability exercise.

The CFL condition establishes a stability bound that links time step and grid spacing for hyperbolic problems, but it does not guarantee convergence quality at finite resolution (Courant et al., 1967). As a result, wavefields can remain numerically stable while accumulating phase delay and amplitude distortion that materially affect interpretation and any downstream sensitivity analysis. The dominant accuracy limitation of low-order explicit finite differences in wave propagation is numerical dispersion. Dispersion error depends strongly on spatial sampling relative to the shortest wavelength in the modeled bandwidth. Reviews of dispersion analysis for explicit finite-difference solvers emphasize that temporal and spatial discretizations jointly shape numerical phase velocity, and that CFL control alone is insufficient as an accuracy criterion (Huang et al., 2024). Methods that intentionally operate at high CFL numbers can remain stable by design, but phase fidelity still requires explicit dispersion control. In near-surface contexts, dispersion is amplified because high frequencies are required to resolve shallow boundaries and thin layers, which increases the minimum-wavelength sampling burden for a fixed grid.

Email: ruhul@tg.itera.ac.id

Recent near-surface and seismic-method developments frequently target dispersion mitigation, either by modifying stencils, optimizing coefficients, or using hybrid strategies that reduce the points-per-wavelength (ppw) requirement for a given error tolerance. A shallow-seismic migration study explicitly frames numerical dispersion suppression as essential for reliable near-surface imaging (Liu et al., 2021). Separately, dispersion-reduction strategies and new FDTD configurations can reduce memory or improve practicality for depth-varying models, but verification of waveform fidelity within the modeled band remains necessary (Wu et al., 2022). High-order or hybrid schemes can achieve acceptable waveform errors with fewer ppw than conventional low-order schemes, but this does not remove the need for explicit accuracy targets and benchmark-based validation (Xu et al., 2025a). The practical implication is that CFL is a necessary operational constraint, while ppw and dispersion analysis provide the accuracy constraint.

This work emphasizes that the novelty is not a new stability or dispersion theory. The contribution is a reproducible near-surface verification framework built around examples and controlled tests. The workflow uses a semi-analytic stratified reference as an independent benchmark, isolates dispersion by varying bandwidth at fixed CFL, and converts correlation-based and norm-based waveform diagnostics into explicit tolerances that define a pass or fail acceptance gate. The objectives are: (i) to demonstrate, using a semi-analytic stratified reference, that CFL-compliant runs can still produce large waveform errors; (ii) to quantify the relationship between ppw, CFL choice, and waveform distortion using correlation-based and norm-based diagnostics; and (iii) to propose a reproducible accuracy checklist for near-surface 1D modeling that treats CFL as a stability gate and ppw plus waveform misfit as accuracy gates.

Method

The variable-density acoustic wave-pressure equation is solved in terms of $V_p(z)$ and $\rho(z)$:

$$\left(\frac{1}{V_p^2(z)}\right)\partial_{tt}p \;-\; \rho(z)\,\partial_z\left[\left(\frac{1}{\rho(z)}\right)\partial_z p\right] \;=\; \rho(z)\,\partial_t q(z,t).$$

The source $q(z,t)$ represents a monopole (isotropic) volume injection implemented through the linearized deformation equation. A standard choice is the zero-phase Ricker wavelet, widely used as a source-time function in wave-equation simulations. One common parameterization is:

$$q(t) \;=\; [1 \;-\; 2\pi^2 {f_0}^2\,(t \;-\; t_0)^2]\; exp[-\pi^2 {f_0}^2\,(t \;-\; t_0)^2],$$

with dominant frequency f_0 and time delay t_0.

Grid dispersion is controlled by enforcing a minimum number of grid points per shortest wavelength $\lambda_{min} = V_{p,min}/f_{max}$, where f_{max} is the effective bandwidth of the source. A practical criterion is:

$$ppw = \frac{\lambda_{min}}{\Delta z} = \frac{V_{p_{min}}}{f_{max}\Delta z} \geq N_{ppw}$$

with N_{ppw} typically set to 10–15 for second-order spatial differencing. The selected ($\Delta z, \Delta t$) pair is therefore jointly determined by the CFL condition and the dispersion constraint. In this report, an intentionally over-resolved case (ppw = 48) is used as a near-converged numerical reference to approximate the layered benchmark as closely as possible. Intermediate ppw values (15–20) are operationally relevant but are not emphasized because the goal is to bracket behavior between insufficient sampling and an over-resolved reference, rather than to optimize a field-practice configuration.

For a second-order explicit scheme in 1D, the Courant–Friedrichs–Lewy (CFL) condition is:

$$\frac{V_{p,max}}{\Delta z}\Delta t \;\leq\; CFL$$

where $V_{p,max}$ is the maximum compressional speed in the model and $CFL \leq 1$ is the stability criteria. In practice, CFL is chosen below unity to accommodate coefficient variation and boundary operators. The selected $(\Delta z, \Delta t)$ pair is therefore jointly determined by the CFL stability bound and the ppw dispersion constraint. For a homogeneous medium and the standard second-order explicit stencil, the discrete dispersion relation satisfies.

$$sin^2\left(\frac{\omega\Delta t}{2}\right) = CFL^2\; sin^2\left(\frac{k\Delta z}{2}\right),$$

Which makes explicit that numerical phase velocity depends on both CFL and the dimensionless sampling $k\Delta z$. In layered media, this relation provides a local diagnostic of dispersion risk as wavelength approaches the grid scale.

Within a layer, the semi-analytic benchmark uses upgoing and downgoing plane waves and expresses propagation over thickness h_j by a 2×2 propagator acting on the state vector, with ordered multiplication through the stack.

$$\mathrm{s}(z_j + h_j) = \mathrm{P}_j(\omega)\,\mathrm{s}(z_j),$$

where $\mathbf{s}(z,\omega) = \begin{bmatrix} p(z,\omega) \\ v(z,\omega) \end{bmatrix}$ and

$$\mathbf{P}_j(\omega) = \begin{bmatrix} cos(k_j\, h_j) & i\, Z_j\, sin(k_j\, h_j) \\ i\left(\frac{1}{Z_j}\right) sin(k_j\, h_j) & cos(k_j\, h_j) \end{bmatrix}.$$

The total propagator from the top of layer 1 to the bottom of layer L is the ordered product $\mathbf{P}(\omega) = \prod_j \mathbf{P}_j(\omega)$. The exact algebraic form of $\mathbf{P}_j$ follows standard acoustic layer matrix constructions and is the report's benchmark backbone. Boundary conditions are chosen to represent a very near-surface acquisition setting.

The top boundary is reflective, which enforces a free-surface condition and preserves surface-related reverberations that are characteristic of shallow layered media. The bottom boundary is absorbing to approximate a semi-infinite half-space and to suppress artificial reflections from the truncated numerical domain. To reduce contamination of dispersion diagnostics by boundary returns, the absorbing layer thickness and domain extension are selected such that any residual bottom-boundary reflections arrive after the primary analysis window $[t_a, t_b]$ at all receiver depths used for verification. However, this paper reports only the relevant domain.

Verification compares the FDTD pressure traces against the semi-analytic layered benchmark at identical receiver depths. Metrics are computed over a selected analysis window $[t_a, t_b]$ that includes the direct arrival and the principal reflections of interest. Define discrete vectors $\mathbf{x} = \{p_{num}(t_a), \dots, p_{num}(t_b)\}$ and $\mathbf{y} = \{p_{ref}(t_a), \dots, p_{ref}(t_b)\}$ containing N_w samples. The residual is $\mathbf{r} = \mathbf{p}_{\text{num}} - \mathbf{p}_{\text{ref}}$. The Euclidean norm is :

$$||\mathbf{x}||_2 = \left(\sum_{i=0}^{N_w-1} x_i^2\right)^{1/2},$$

and the infinity norm is $||\mathbf{x}||_\infty = \max_i |x_i|$.

Residual traces are used to evaluate relative norms over an analysis window. The following metrics separate energy misfit (L2) from peak mismatch (L∞):

$$\mathbf{E}_2 = \frac{||\mathbf{r}||_2}{||\mathbf{p}_{\text{ref}}||_2}, \qquad \mathbf{E}_\infty = \frac{||\mathbf{r}||_\infty}{||\mathbf{p}_{\text{ref}}||_\infty}.$$

The normalized cross-correlation between x and y at integer lag $\mathfrak{L}$ is

$$c(\mathfrak{L}) = \frac{\sum_{i=0}^{N_w-1} x_i\, y_{i-\mathfrak{L}}}{||\mathbf{x}||_2\, ||\mathbf{y}||_2}, \qquad \mathfrak{L}^* = \arg\max_{\mathfrak{L} \in [-L,L]} c(\mathfrak{L}),$$

where $y_{i-\mathfrak{L}}$ is interpreted as zero outside the window.

The report computes the lag maximizing normalized cross correlation and also reports a zero lag correlation coefficient as a shape metric:

$$r_0 = \frac{\mathbf{p}_{\text{num}} \cdot \mathbf{p}_{\text{ref}}}{||\mathbf{p}_{\text{num}}||_2\, ||\mathbf{p}_{\text{ref}}||_2},$$

where · denotes the dot product. Lag captures kinematic agreement independent of amplitude scaling, while r_0 penalizes phase errors without time shifting.

Explicit tolerances (lag, relative norms, correlation) declare that the solver configuration validated only if all receivers pass within the primary analysis window.

Experimental setup

A 1D layered medium is defined on the depth coordinate z (m), positive downward. The total model depth is z_max = 39 m. A uniform spatial grid with spacing Δz = 0.1 m is used, giving Nz = 391 grid samples. Each layer is assigned constant density ρ (kg m^{-3}) and compressional wave speed Vp (m s^{-1}).

Layer 1: thickness 2 m, ρ = 1600, Vp = 600
Layer 2: thickness 6 m, ρ = 1500, Vp = 1800
Layer 3: thickness 1 m, ρ = 1550, Vp = 2200
Layer 4: thickness 10 m, ρ = 1700, Vp = 2800
Layer 5: thickness 20 m, ρ = 2300, Vp = 4500

The velocity extrema used in stability and resolution checks are $V_{p_{min}}$ = 600 m s^{-1} and $V_{p_{max}} = 4500$ m s^{-1}.

A colocated surface-source configuration is used to stress shallow reverberations and interface scattering. The monopole source is positioned at $z_s = 0.0\, m$, snapped to grid index $i_s = 0$ (0-based indexing). Pressure receivers are sampled at the following grid-snapped depths:

r1: z = 0.0 m (i = 0)
r2: z = 1.9 m (i = 19)
r3: z = 7.9 m (i = 79)
r4: z = 9.1 m (i = 91)
r5: z = 14.0 m (i = 140)
r6: z = 24.0 m (i = 240)

This depth distribution captures both early-time near-surface responses and later arrivals influenced by deeper propagation and internal multiples.

Two experimental scenarios are designed to separate numerical stability from numerical accuracy in 1D acoustic finite-difference time-domain (FDTD) modeling. Stability is controlled by enforcing an identical Courant–Friedrichs–Lewy (CFL) number in both experiments. Accuracy is perturbed by changing the effective maximum frequency used for verification.

This change alters the minimum wavelength and therefore the ppw at fixed spatial grid spacing. The layered model, spatial grid, boundary physics, receiver geometry, dominant source frequency, and CFL target are held constant so that differences in waveform agreement can be attributed to dispersion-related resolution.

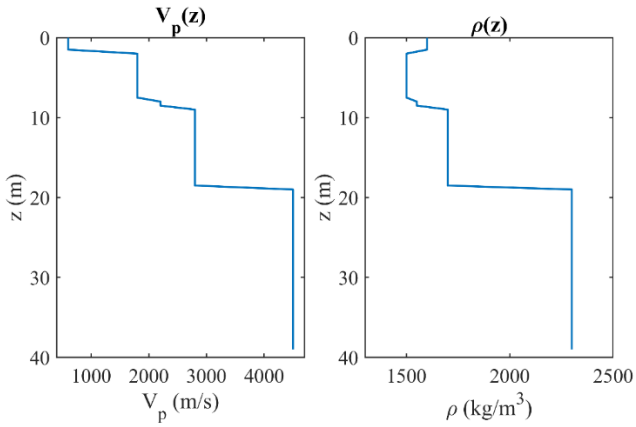

Figure 1. Layer properties used in modelling as a function of depth, Left: $\boldsymbol{V_p(z)}$ and Right: $\boldsymbol{\rho(z)}$.

Stability is measured by the CFL number: $CFL = Vp_{max}\,\Delta t\,/\,\Delta z$, with Vp_max = 4500 m s^{-1}, Δt = 2 × 10^{-6} s, and Δz = 0.1 m, both experiments satisfy $CFL \approx 0.10$.

Resolution is measured by points per minimum wavelength:

$$ppw = \frac{\lambda_{min}}{\Delta z}, \text{ with } \lambda_{min} = \frac{Vp_{min}}{f_{max}}.$$

Experiment 1: λ_min = 0.96 m, ppw = 9.6.
Experiment 2: λ_min = 4.8 m, ppw = 48.

Therefore, both experiments are CFL-stable, but only Experiment 2 is strongly over-resolved relative to the modeled bandwidth.

Result and Discussion

Both simulations were CFL-stable (CFL = 0.100), yet the accuracy outcome changed from universal failure to universal pass as *ppw* increased from 9.6 to 48. This demonstrates that CFL compliance cannot be used as an accuracy proxy for near-surface modeling. The controlled change in f_{max} alters the minimum wavelength and therefore *ppw* at fixed Δz. The metrics show strong sensitivity to *ppw* , consistent with numerical dispersion as the dominant error mechanism. Low *ppw* produces depth-growing timing bias and large amplitude misfits. High *ppw* suppresses distortion and yields acceptable waveform agreement.

Experiment 1 shows that zero-lag correlation above 0.96 can coexist with unacceptable L2 and Linf norms (Table 1). Therefore, accuracy claims require a multi-metric acceptance gate that combines kinematic and amplitude-sensitive diagnostics. Experiment 2 shows that when *ppw* is high, all metrics jointly support acceptance (Table 2).

The paired experiments provide a controlled demonstration that CFL compliance is a stability condition rather than an accuracy guarantee. This separation between stability and dispersion error is consistent with modern analyses of explicit finite-difference wave solvers, where the time step primarily governs stability while spatial sampling governs numerical dispersion and phase error (Courant et al., 1967; Huang et al., 2024). Both runs used identical spatial sampling (Δz = 0.1 m) and the same CFL target (v ≈ 0.1), yet the verification outcome changed from universal failure (Experiment 1) to universal pass (Experiment 2) when points per minimum wavelength increased from 9.6 to 48.

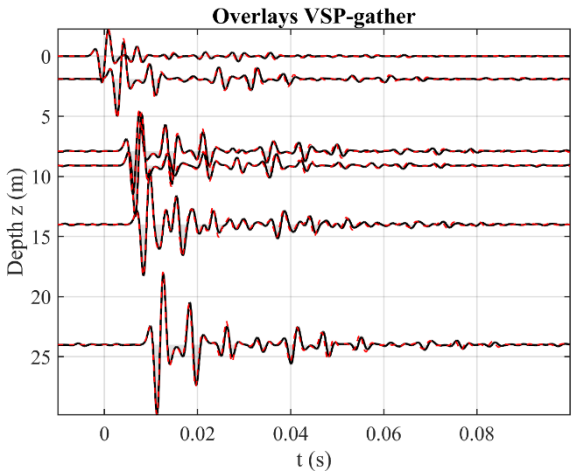

Figure 2. Numerical (dashed-red) vs Physical (solid-black) from Experiment 1.

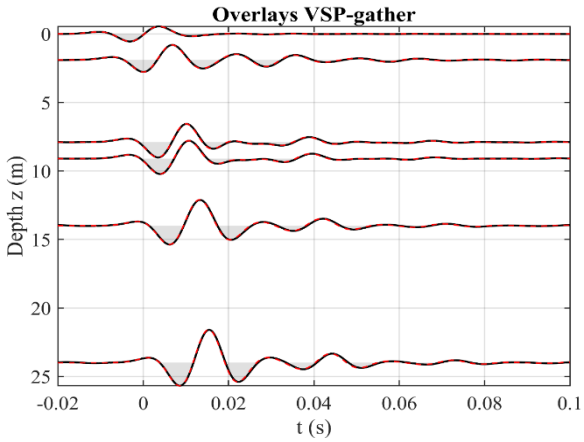

Figure 3. Numerical (dashed-red) vs Physical (solid-black) from Experiment 2.

This isolates numerical dispersion as the dominant mechanism separating stable-but-inaccurate

solutions from stable-and-acceptable solutions in the layered near-surface setting. The implication is that a CFL-only configuration rule can yield synthetics that are stable and reproducible but systematically biased, especially when high-frequency content is present (Rao & Wang, 2019).

Tabel 1. Verification metrics for Experiment 1

Experiment 1						
Receiver	**Lag_samples**	**Lag_seconds**	**L2**	**Linf**	**ZeroLagCorr**	**PASS**
1	-12	-2.6667e-05	0.1705	0.092061	0.98608	false
2	-34	-7.5556e-05	0.26967	0.16622	0.96778	false
3	-44	-9.7778e-05	0.28675	0.20388	0.96196	false
4	-30	-6.6667e-05	0.21291	0.12395	0.97795	false
5	-41	-9.1111e-05	0.26172	0.17837	0.96628	false
6	-41	-9.1111e-05	0.26428	0.18361	0.96562	false
[STATUS] FAIL						

Tabel 2. Verification metrics for Experiment 2

Experiment 2						
Receiver	**Lag_samples**	**Lag_seconds**	**L2**	**Linf**	**ZeroLagCorr**	**PASS**
1	0	0	0.013695	0.0092701	0.99991	true
2	-66	-0.00014667	0.013695	0.056419	0.99672	true
3	-58	-0.00012889	0.071129	0.053464	0.99748	true
4	-56	-0.00012444	0.066391	0.049163	0.99779	true
5	-69	-0.00015333	0.078054	0.054413	0.99695	true
6	-68	-0.00015111	0.080584	0.054472	0.99675	true
[STATUS] PASS						

Experiment 1 produced zero-lag correlations between 0.962 and 0.986 while still failing at all receivers due to large L2 and L∞ misfits and non-trivial timing lags. This pattern is diagnostic. Normalized correlation metrics can remain high when gross waveform character is preserved, even if dispersion perturbs phase and relative amplitude sufficiently to violate quantitative accuracy targets (Tao et al., 2017; Gao et al., 2023). The magnitude of optimal lag generally increased with receiver depth to approximately 10^{-4} s by $z \geq 7.9$ m. This behavior is consistent with cumulative dispersive delay, where phase-velocity error accrues with propagation distance and with repeated reflections.

Theoretical and computational discussions of dispersion in explicit finite-difference schemes identify spatial sampling (points per wavelength) as a dominant control on phase error, and emphasize that error accumulation becomes more consequential as wave paths lengthen and become more complex. Layering intensifies accumulation because each interface generates transmitted and reflected components that traverse the medium multiple times. Accuracy requirements for near-surface modeling should therefore be set by worst-case path complexity rather than by a single first-arrival offset.

Experiment 2 passed all receivers under the tolerances defined here, while deeper receivers retained negative lags of order 1.3×10^{-4} s to 1.5×10^{-4} s. This is consistent with common verification practice where a time-shift diagnostic is treated separately from amplitude and waveform-shape acceptance, particularly when the principal goal is waveform similarity rather than strict phase alignment. The broader FWI misfit literature highlights that time-shift and correlation-based measures can tolerate small systematic shifts while remaining useful for controlling cycle skipping and stabilizing comparisons (Gao et al., 2023). For applications requiring phase-accurate synthetics, lag tolerances should be explicitly tightened, or dispersion mitigation should be introduced through higher-order or optimized schemes (Xu et al., 2025). Near-surface studies often depend on subtle amplitude ratios, phase differences, and polarity changes associated with thin layers and strong contrasts. In the ppw = 9.6 regime, relative L2 errors reached approximately 0.29 and relative peak errors reached approximately 0.20. These error levels are large enough to map numerical artifacts into apparent geological sensitivity, especially when comparing small model perturbations. Dispersion-suppression strategies in near-surface contexts are explicitly motivated by this risk, including migration and modeling workflows that target reduced dispersion contamination (Liu et al., 2021). Methodologically, recent work on optimized finite-difference operators demonstrates that dispersion budgets can be enforced more efficiently by stencil optimization, lowering the

points-per-wavelength requirement for a given phase-velocity error threshold (Xu et al., 2025). The experiments therefore support a procedural recommendation: CFL checks should be reported as stability gates, but accuracy should be enforced through dispersion-aware parameters defined for the slowest velocity and the highest relevant frequency, then verified against an independent benchmark using multi-metric criteria (Huang et al., 2024; Rao & Wang, 2019; Xu et al., 2025).

The pass–fail limits are operational and benchmark-referenced rather than universal. They are defined for a fixed layered model, fixed boundary-condition design, and a fixed source band used in the verification runs. The sensitivity of the acceptance decision to systematic variations in source bandwidth, impedance contrast, and CFL value is therefore not exhaustively characterized in this report. The intent is to isolate the stability–accuracy gap by holding CFL and model structure fixed while varying numerical resolution and then translating waveform misfits into an explicit dispersion budget. The same verification workflow is directly extensible to factorial sweeps in (ppw, CFL, f_{max} , contrast), which would support broader generalization through error–parameter response surfaces.

The boundary-condition residual statistic was substantially larger in Experiment 1 than in Experiment 2. This suggests that at marginal resolution, boundary enforcement interacts with dispersion and layered scattering to amplify numerical artifacts. Reviews of perfectly matched layer methodology emphasize that boundary treatments have coupled impacts on accuracy and stability, and that numerical implementations can become more delicate when broadband or high-frequency numerical content is generated near boundaries (Pled & Desceliers, 2022). Since the benchmark radiation residual was at machine precision, the residual mismatch primarily reflects the discrete implementation, including discretization near the free surface and source collocation. More broadly, modern formulations that improve interface and free-surface treatment still report CFL-governed stability while targeting improved accuracy with fewer points per wavelength, underscoring the same stability–accuracy distinction highlighted by these experiments.

The experiments are intentionally 1D and therefore isolate dispersion and interface scattering without lateral heterogeneity or mode conversion. This limitation does not weaken the core conclusion, because 1D is a favorable setting for finite differences. A scheme that fails fidelity in 1D layered reverberations is unlikely to improve in higher-dimensional near-surface settings. Targeted extensions include: testing higher-order or dispersion-optimized stencils to reduce ppw requirements; varying source placement relative to the free surface; comparing alternative bottom absorbing conditions guided by modern PML analyses; adding systematic sweeps over source bandwidth, impedance contrast, and CFL; and adding frequency-domain phase and amplitude diagnostics to attribute misfit to dispersion more directly, consistent with contemporary misfit-function frameworks used in waveform inversion and validation.

Conclusion

The experiments establish a clear separation between numerical stability and numerical accuracy for 1D acoustic FDTD in a layered near-surface setting. The experiments validate the central thesis: CFL compliance is necessary for stability but insufficient for accuracy. Waveform fidelity is governed primarily by dispersion budget, controlled by ppw , bandwidth, and discretization order, and must be validated against an independent benchmark using multiple complementary metrics. A methodological implication follows for near-surface forward modeling. CFL should be treated as a stability gate, while accuracy should be enforced through an explicit dispersion design requirement, expressed as points per wavelength for the slowest velocity and the highest relevant frequency, and validated by multi-metric waveform comparisons to an independent benchmark. This framing reduces the risk of interpreting numerical artefacts as geologic sensitivity and supports defensible forward modeling for near-surface applications.

Acknowledgements

The authors thanks reviewers for their insightful comments.

References

Courant, R., Friedrichs, K., & Lewy, H. (1967). On the partial difference equations of mathematical physics. IBM Journal of Research and Development, 11(2), 215–234. https://doi.org/10.1147/rd.112.0215

Gao, Y., Tilmann, F., & Rietbrock, A. (2023). A review of misfit functions for adjoint full waveform inversion in seismology. Geophysical Journal International, 235(3), 2794–2827. https://doi.org/10.1093/gji/ggad372

Huang, J.-P., Peng, W.-T., Yang, J.-D., & Lou, L.-F. (2024). Overview of computation strategies on the dispersion analysis for explicit finite difference solution of acoustic wave equation. Petroleum Science, 21(4), 2311–2328. https://doi.org/10.1016/j.petsci.2024.02.003

Kelly, K. R., Ward, R. W., Treitel, S., & Alford, R. M. (1976). Synthetic seismograms: A finite-

difference approach. Geophysics, 41(1), 2–27. https://doi.org/10.1190/1.1440605

Liu, Y., Li, Z., Wang, J., Sun, M., & Liu, Q. (2021). A numerical dispersion-suppressed method for shallow seismic migration. Near Surface Geophysics, 19(1), 109–121. https://doi.org/10.1002/nsg.12134

Pled, F., & Desceliers, C. (2022). Review and recent developments on the perfectly matched layer (PML) method for the numerical modeling and simulation of elastic wave propagation in unbounded domains. Archives of Computational Methods in Engineering, 29, 471–518. https://doi.org/10.1007/s11831-021-09581-y

Rao, Y., & Wang, Y. (2019). Dispersion and stability condition of seismic wave simulation in TTI media. Pure and Applied Geophysics, 176, 1549–1559. https://doi.org/10.1007/s00024-018-2063-y

Tao, K., Grand, S. P., & Niu, F. (2017). Full-waveform inversion of triplicated data using a normalized-correlation-coefficient-based misfit function. Geophysical Journal International, 210(3), 1517–1524. https://doi.org/10.1093/gji/ggx249

Wu, B., Tan, W., Xu, W., & Li, B. (2022). Trapezoid-grid finite-difference time-domain method for 3D seismic wavefield modeling using CPML absorbing boundary condition. Frontiers in Earth Science, 9, Article 777200. https://doi.org/10.3389/feart.2021.777200

Xu, Q., Jin, C., Liang, K., & Cao, D. (2025). An optimized 13-point finite-difference operator for 2D frequency-domain acoustic wave modeling. Journal of Geophysics and Engineering, 22(4), 971–985. https://doi.org/10.1093/jge/gxaf051